HEPCAT First Year Progress Report

Jianyang Qi (University of California, San Diego)

1 Introduction

The first year of my HEPCAT fellowship was primarily spent on two topics: the development and characterization of the Liquid Xenon Proportional Scintillation Counter (LXePSC) at the University of California, San Diego (UCSD), and the improvement of the detector subsystems of the xenon-doped liquid argon (LAr) setup, named CHILLAX [1], at Lawrence Livermore National Laboratory (LLNL). The results of the LXePSC were submitted to the Journal of Instrumentation, and uploaded to the arXiv [2]. As such, the discussion of my work on the LXePSC will draw heavily from our paper, with some technical details left out.

2 Development of the Liquid Xenon Proportional Scintillation Counter

2.1 LXePSC with different anode wire diameters

Liquid xenon time projection chambers (LXeTPCs) work by detecting the prompt scintillation signal (S1), and the delayed ionization signal (S2) of an energy deposition. The LXePSC is a cylindrical LXe target where the S2 is produced near an anode wire in the center of the detector. Twenty cathode wires are at the edge of the sensitive LXe target and simultaneously act as a shield for the Photomultiplier Tubes (PMTs). The current design is a modification to the LXePSC designed by our former staff scientist, Yuehuan Wei, which used a 25 μm diameter anode wire [3], and an L-shaped anode holder at the top and bottom of the detector (see Fig. 1 of [3]). We replaced the L-shaped anode holder at the top and bottom of the detector with Accu-Glass Push-On 0.040 connectors, and the 25 μm diameter anode wire with a 10 μm diameter wire (both are gold-plated tungsten wires from California Fine Wire Co.). This is to investigate whether we can get a higher gain of photons per electron, as we can achieve a larger maximum electric field with a thinner wire given a fixed anode-to-cathode voltage. These modifications can be seen in Fig. 1.

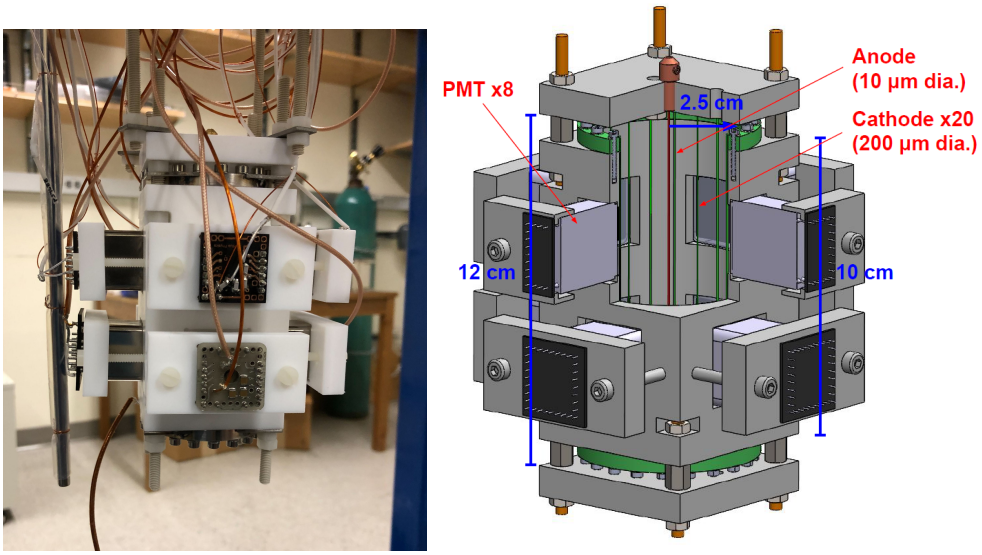

Figure 1: **Left**: A picture of the LXePSC during the installation of the 10 μm diameter anode. **Right:** The design drawing of the detector. The wire diameters are scaled up so that they are visible.

2.2 New Software Framework

2.2.1 Data Taking

One of the primary issues with our previous run [3] was peak-finding with high levels of light emission. This peak-finding used to be done on the waveform summed across all channels, which is much noisier than the per-channel waveforms. As such, I wrote a new data processor such that above-threshold *per-channel* pulse hits were found first, then summed across channels into *peaks*. Similar to the two-phase xenon TPCs, the S1 and S2 signals have different waveform shapes in the LXePSC. The S1 shape looks like two decaying exponentials due to de-excitation, and the S2 shape looks approximately gaussian due to the diffusion of electrons. S1s and S2s are then classified based on the waveform shape, and grouped into *events* (see Fig. 3 for an example). The processed data was saved into `numpy` structured arrays, which is basis for our data-analysis framework.

2.2.2 Simulations

As with any experiment, we needed to model the non-idealities of our detector in order to better understand the detector response and to estimate systematic uncertainties. Our electric field, in particular, faced many deviations from a perfect $\sim 1/r$ electric field, such differing PMT voltages, and cathode-wire bending. We used COMSOL™ multiphysics to model the electric field within our detector with these non-ideal conditions in mind. In addition, I wrote a package to feed the output of the electric field simulation into our analysis framework, which allowed for fast interpolation of the electric field on a cylindrical grid. Our field simulations are summarized in Fig. 2.

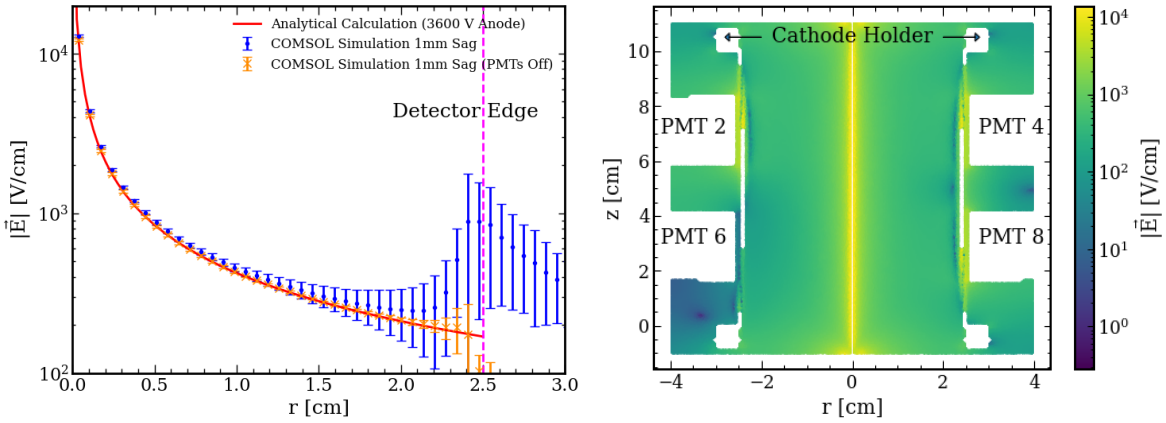

Figure 2: **Left:** The electric field as a function of r for the central 2.47 cm (in z) of the detector. The error bars refer to the standard deviation of the electric field in z and θ at a particular r. This simulation assumes a 3600 V anode, grounded cathode, and PMTs at their operating voltages. The simulated electric field from COMSOL is larger than the analytic calculation, due to the effect of the negative high voltage PMTs being near the grounded cathode. When the PMTs are grounded, this effect goes away and the field is more consistent with the analytical calculation. **Right:** A map of the magnitude of the electric field for a slice along the $r - z$ plane. The electric field was simulated using COMSOL™ multiphysics for both figures.

In addition to the electric field, we modelled the response of external radiation sources that we use to calibrate our detector, such as ^{137}Cs. These external sources produce energy depositions that are not uniformly distributed in our detector, and thus must be determined by simulation as we do not have a full 3-D position reconstruction. To do this, I developed the GEANT4 simulation for our detector.

2.3 Detector calibration with ^{137}Cs

To calibrate the response of the detector, we need to see the S1 and S2 response of a monoenergetic source. This equates to finding the average light collection efficiency and ionization gain (photoelectrons detected per electron), also known as g_1 and g_2. We used a ^{137}Cs, 661.7 keV gamma source placed in a cup on the outer vessel of the detector, and vertically aligned near the middle of the detector. In our previous run, we achieved $g_1 = 0.13$ PE/γ and $g_2 = 0.7$ PE/e$^-$ with all eight PMTs turned on, and with a 4 kV anode and -750 V cathode; this corresponds to an anode-surface field of 495 kV/cm [3]. Furthermore, the ^{137}Cs photopeak was smeared significantly, to the point where a calibration was difficult to achieve with any voltages greater than 4 kV. In this run, we were able to achieve a higher g_2 of 1.6 ± 0.2 PE/e$^-$ at an anode voltage of 3.6 kV. Considering g_1, this value of 1.6 PE/e$^-$ corresponds to ~ 17 photons produced by electroluminescence in the liquid. It is important to note that this g_2 is denoted as the *ionization gain* rather than the single-electron gain. Although there is no incomplete extraction, we expect a small effect from the electron-lifetime, so the size of the S2 from the ^{137}Cs peak is only comprised of the ionization electrons which did not attach to impurities. As such, g_2 is an underestimation of the single-electron gain. Furthermore, we were able to sweep the g_1 and g_2 values across multiple anode voltages. At above 3.6 kV on the anode, we start to observe spurious light emission.

In dual phase LXeTPCs, g_1 and g_2 are estimated via calibrations using multiple monoenergetic sources. However, we only had the ^{137}Cs source available to us at this time, so we estimate our g_1 and g_2 by finding $g_1 = S1_c/\langle n_\gamma \rangle$ and $g_2 = S2_c/\langle n_e \rangle$. $S1_c$ and $S2_c$ are the mean $S1$ and $S2$ values of the ^{137}Cs photopeak, and are found by applying several data quality cuts as described in [2]. n_γ and n_e are the number of S1 (S2) photons (electrons) given by the Noble Element Simulation Technique (NEST) [4], which takes the electric field and deposited energy as input. The deposited energy is simply 661.7 keV, however, to find the electric field, we must first get the position of the events, followed by a multi-step simulation chain, also described in [2].

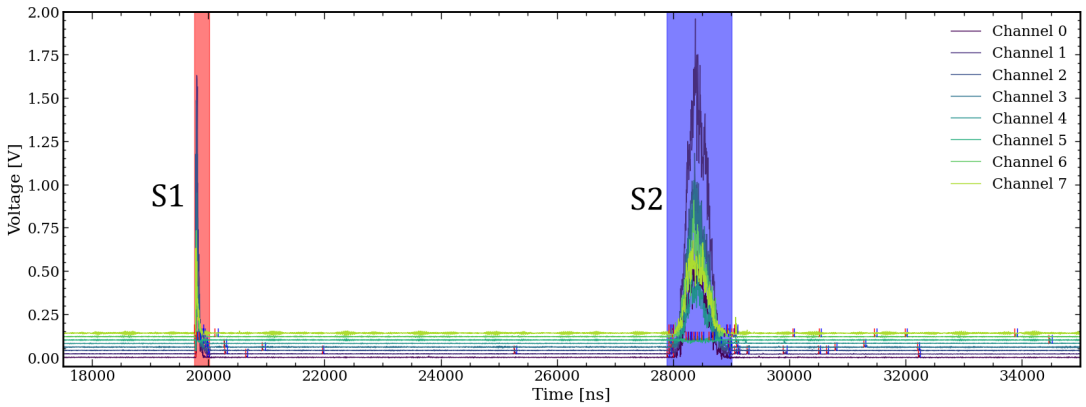

Figure 3: Example waveform for a ^{137}Cs event for 3 kV anode and grounded cathode. S1 highlighted in red, S2 highlighted in blue.

2.4 Detection of Low-energy Electronic Recoils from Tritium

We injected a tritiated methane source into our detector in order to probe the response to low energy electron recoils (ER) of a few keV. These events populate a band in $(S1, \log(S2/S1))$ space (Fig. 6), and we can count the rate of these events in the band as a function of time. During this calibration, the anode was at a voltage of 3600 V. The tritiated methane was removed from the detector by the SAES getter in the gas circulation loop over the course of three days. This is the first detection of electronic recoils down to 1 keV in a single-phase LXe

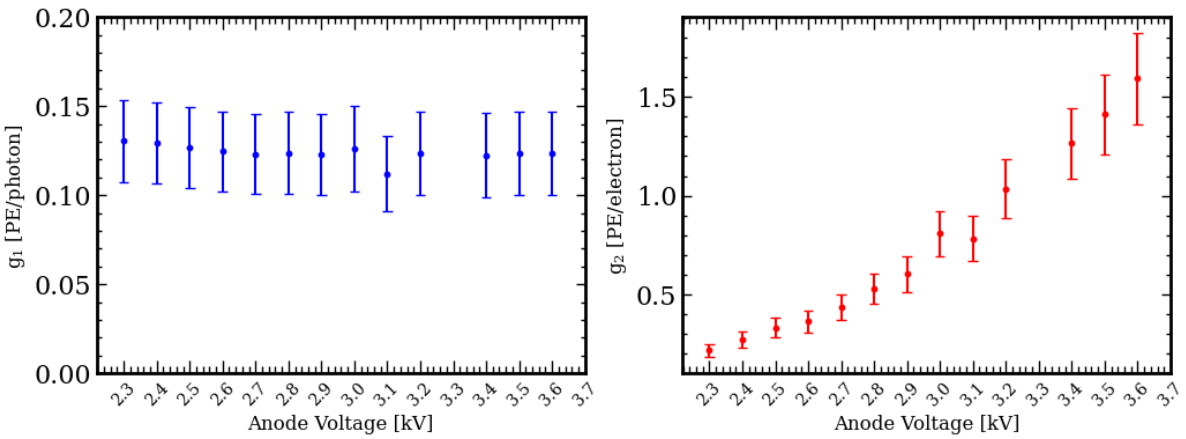

Figure 4: g_1 and g_2 for the values of the voltage sweep. Systematic uncertainty comes from the possible positions of the ^{137}Cs source, the photopeak selection in S2 vs S1 space, the electric field configuration, and from the NEST systematic errors.

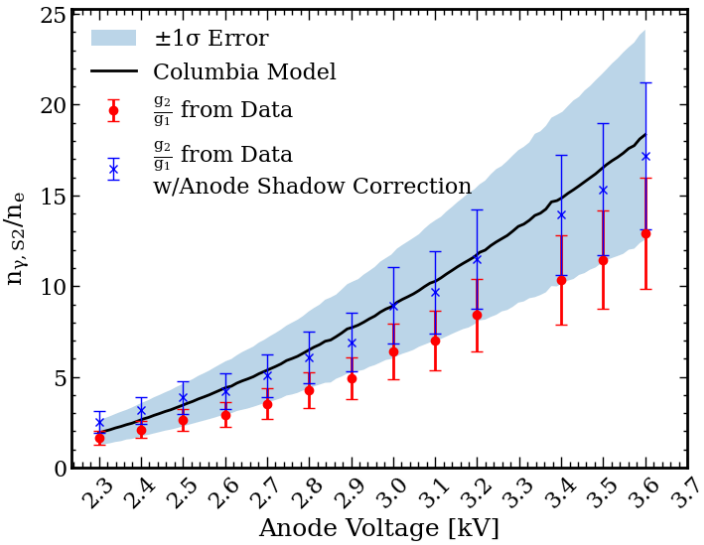

Figure 5: A comparison of electroluminescence yield n_γ/n_e to the Columbia model [5]. We see that up to 17±4 photons are produced per electron at an anode voltage of 3.6 kV. The upper limit of n_γ/n_e is given by correcting the effect of the anode blocking some of the S2 light. The 1σ shaded region is computed by sampling the parameters given in the Columbia model with their associated uncertainties.

detector using both light and charge information.

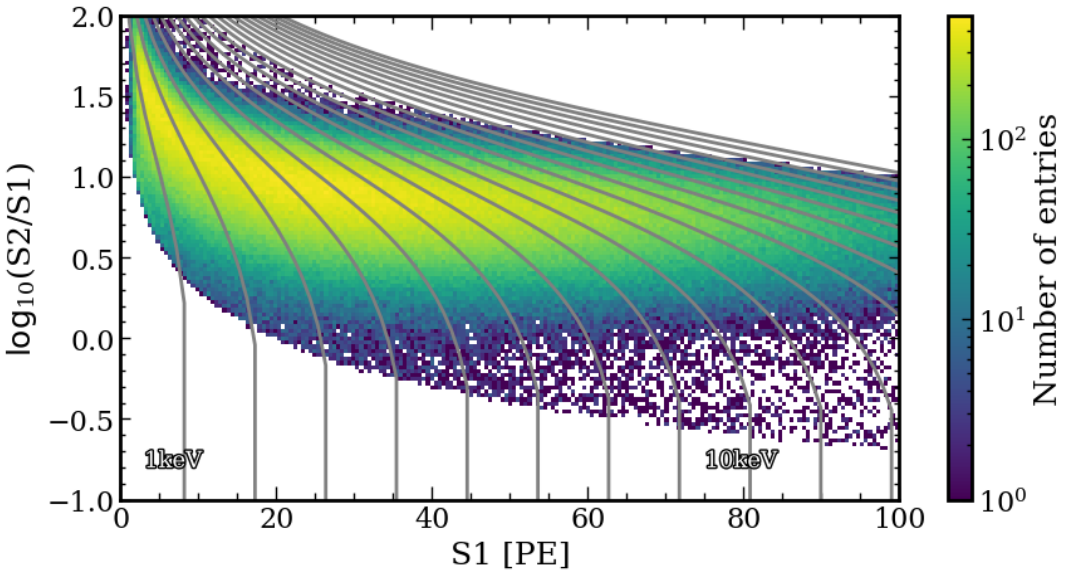

Figure 6: The low energy ER band from the tritium events after applying the aforementioned cuts. The gray lines are approximate energy contours in 1 keV.

3 Improvements to the CHILLAX Subsystems

During my first year as a HEPCAT fellow, I spent the summer of 2022 working at LLNL under the supervision of Jingke Xu. Here, I learned about the CHILLAX setup and xenon-doping of liquid argon, and helped to improve its various systems. These improvements will be useful in the next step of CHILLAX, which involves placing a time projection chamber (TPC) inside of the cryostat. First, I fixed a stability issue in the slow-control system, which required it to be restarted once every few weeks. In addition, I implemented a graphical interface which allows for live-time monitoring and plotting of the system variables. Secondly, I helped to manufacture the high voltage feedthroughs, to be used in CHILLAX, under the guidance of project scientist, Ethan Bernard. This is important as TPCs rely on drifting electrons through an electric field, which will require a system to deliver high voltages (several kV) to the TPC electrodes. Lastly, the previous data-acquisition system could only use a single digitizer board, which limits the number of readouts that a detector can have. To fix this issue, I learned to synchronize and program the communication between digitizer boards, and now the data acquisition system can synchronously read and write to multiple boards at once. This will be useful as a detector with more photosensors can have a higher position resolution compared to a detector with fewer, and improved position resolution is a potential benefit to the xenon-doped argon compared to bare argon.

References

[1] Ethan P. Bernard et al. "Thermodynamic Stability of Xenon-Doped Liquid Argon Detectors". In: (Sept. 2022). arXiv: 2209.05435 [physics.ins-det].

[2] Jianyang Qi et al. "Low Energy Electronic Recoils and Single Electron Detection with a Liquid Xenon Proportional Scintillation Counter". In: (Jan. 2023). arXiv: 2301.12296 (physics.ins-det).

[3] Yuehuan Wei et al. "Performance of a radial time projection chamber with electroluminescence in liquid xenon". In: *JINST* 17.02 (2022), p. C02002. DOI: 10.1088/1748-0221/17/02/C02002. arXiv: 2111.09112 [physics.ins-det].

[4] M. Szydagis et al. *Noble Element Simulation Technique*. Version v2.3.11. Sept. 2022. DOI: 10.5281/zenodo.7061832. URL: https://doi.org/10.5281/zenodo.7061832.

[5] E. Aprile et al. "Measurements of proportional scintillation and electron multiplication in liquid xenon using thin wires". In: *JINST* 9.11 (2014), P11012. DOI: 10.1088/1748-0221/9/11/P11012. arXiv: 1408.6206 [physics.ins-det].